CHEMISTRY OF MATERIALS
Article

Chem. Mater. **2011,** *23,* 163–170 163
DOI:10.1021/cm102592p

Spontaneous Superlattice Formation in the Doubly Ordered Perovskite $KLaMnWO_6$

Susana Garcia-Martin,*[,†] Graham King,[‡,§] Esteban Urones-Garrote,[†] Gwilherm Nénert,[⊥] and Patrick M. Woodward*[,‡]

[†]*Departamento de Química Inorgánica, Facultad de Ciencias Químicas, Universidad Complutense, Madrid 28040, Spain,* [‡]*Department of Chemistry, The Ohio State University, 100 West 18th Avenue, Columbus, Ohio 43210-1185, United States , and* [⊥]*Institut Laue-Langevin, 6 rue Jules Horowitz, 38042 Grenoble Cedex 9, France.* [§]*Current address: Lujan Neutron Scattering Center, Los Alamos National Laboratory, MS H805, Los Alamos, NM 87545, USA*

Received September 9, 2010. Revised Manuscript Received November 10, 2010

Electron, neutron, and synchrotron X-ray diffraction together with transmission electron microscopy studies reveal the spontaneous formation of a complex superlattice in bulk samples of the perovskite $KLaMnWO_6$. The superlattice structure, which possesses $P\bar{4}2m$ space group symmetry with $a = 40.0637(7)$ Å and $c = 8.1306(3)$ Å, results from a two-dimensional compositional modulation of the *A*-site cations (K^+ and La^{3+}), combined with a complex pattern of tilts involving the corner connected octahedra. The basic pattern of octahedral tilting involves out-of-phase tilts of neighboring octahedra about the pseudocubic *a* and *b* axes ($a^-a^-c^0$ tilting). Unexpectedly, the out-of-phase tilting is disrupted in both directions by an in-phase tilt once every five octahedra. The occurrence of regularly repeating, well-separated in-phase tilts helps to alleviate strains that arise from formation of the compositionally modulated chessboard superlattice.

1. Introduction

There is a growing interest in the study of superlattices and self-assembled nanostructures due to their potential use in multifunctional integrated systems. Complex superlattice structures can be prepared using methods such as pulsed laser deposition or molecular beam epitaxy.[1−3] The novel properties of superlattices are attractive, but the vacuum deposition techniques used to produce well ordered patterns are expensive. An alternate approach is to use simple wet-chemistry techniques to achieve nanometer-scale self-assembly of materials. Although this approach is more economical, the resulting superlattice structures are often irregular and nonperiodic. A third approach is to find compositions that spontaneously form periodic superlattices at high temperature using standard solid-state synthetic methods. Interesting examples of solid-state self-assembly have recently been found in oxide systems.[4−6]

We have previously reported spontaneous superlattice formation in $NaLaMgWO_6$.[7] This perovskite material forms a modulated structure consisting of alternating La-rich and La-poor stripes, each $6a_p$ unit cells wide, where a_p is the unit cell of the simple cubic perovskite structure (~4 Å). The resulting superlattice repeats with a $12a_p$ periodicity along either the $[100]_p$ or the $[010]_p$ direction. The La-rich and La-poor stripes are thought to have nominal stoichiometries of $(La_xNa_{1-3x})LaMgWO_6$ and $NaLaMgWO_6$, respectively. Other examples of spontaneous compositional nanopatterning in perovskites have been reported in the literature.[6,8,9] Both chessboard and stripe ordered superstructures, as well as a mixture of the two, have been reported.

For perovskites the tolerance factor, τ, gives a measure of the fit of the larger *A*-site cation to the cubic framework of corner connected octahedra. When τ falls below unity, as is the case for $NaLaMgWO_6$ where $\tau = 0.952$, octahedral tilting distortions are expected.[10] Neutron diffraction studies of $NaLaMgWO_6$ revealed an unexpectedly complex pattern of octahedral tilting. The basic pattern of tilting in $NaLaMgWO_6$ involves out-of-phase tilting of neighboring octahedra about the *a* and *b* axes of the pseudocubic perovskite unit cell. This pattern, denoted as $a^-a^-c^0$ tilting in the standard Glazer notation, is not a very common tilt system at room temperature, but is

*Corresponding author. E-mail: sgmartin@quim.ucm.es (S.G.-M.); woodward@chemistry.ohio-state.edu (P.M.W.).

(1) Lee, H. N.; Christen, H. M.; Chisholm, M. F.; Rouleau, C. M.; Lowndes, D. H. *Nature* **2005**, *433*, 395.
(2) Ziese, M.; Setzer, A.; Vrejoiu, I.; Birajdar, B. I.; Rodríguez, B. J.; Hesse, D. *J. Appl. Phys.* **2008**, *104*, 06398.
(3) Bousquet, E.; Dawber, M.; Stucki, N.; Lichtensteiger, C.; Hermet, P.; Gariglio, S.; Triscone, J. M.; Ghosez, P. *Nature* **2008**, *452*, 732.
(4) Zhang, C. L.; Yeo, S.; Horibe, H.; Choi, Y. J.; Guha, S.; Croft, M.; Cheong, S. W. *Appl. Phys. Lett.* **2007**, *90*, 133123.
(5) Zhang, C. L.; Tseng, C. M.; Chen, C. H.; Yeo, S.; Choi, Y. J.; Cheong, S. W. *Appl. Phys. Lett.* **2007**, *91*, 233110.
(6) Guiton, B. S.; Davies, P. K. *Nat. Mater.* **2007**, *6*, 586.
(7) García-Martín, S.; Urones-Garrote, E.; Knapp, M. C.; King, G.; Woodward, P. M. *J. Am. Chem. Soc.* **2008**, *130*(45), 15028.
(8) Guiton, B. S.; Davies, P. *J. Am. Chem. Soc.* **2008**, *130*, 17168.
(9) Lu, J. B.; Yang, H. X.; Li, Z. A.; Ma, C.; Shi, H. L.; Zeng, L. J.; Li, J. Q. *J. Solid State Chem.* **2008**, *181*, 3194.
(10) Woodward, P. M. *Acta Crystallogr., Sect. B* **1997**, *53*, 44.

Published on Web 12/17/2010

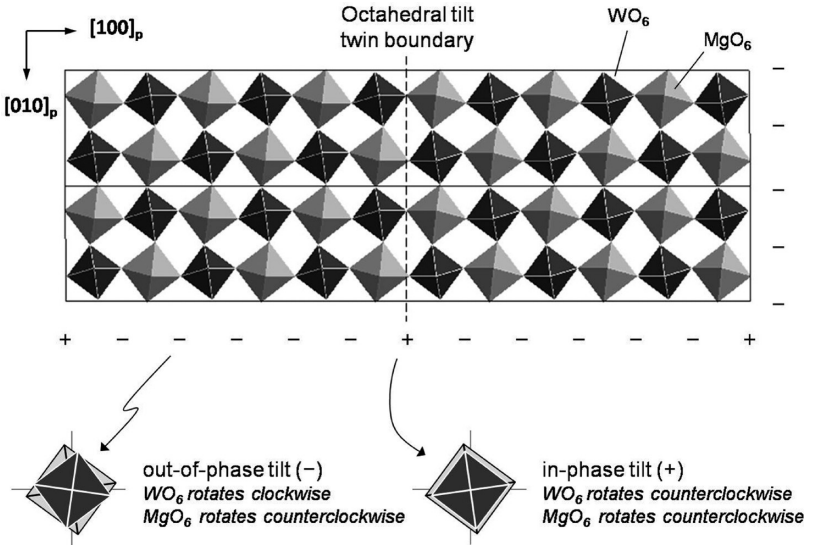

Figure 1. Octahedral tilting in $NaLaMgWO_6$. The − and + symbols indicate out-of-phase and in-phase octahedral tilting, respectively. The Na^+ and La^{3+} ions are omitted for clarity.

known to occur in a number of perovskites, including Ba_2MBiO_6 (M = Tb, Pr, Nd) and Sr_2NiTeO_6.[11] The unusual aspect of tilting in $NaLaMgWO_6$ is the presence of in-phase tilts about the a-axis (but not the b-axis) once every six octahedra (Figure 1).[12] This rare type of octahedral tilting is sometimes referred to as octahedral tilt twinning, where the in-phase tilts are treated as a type of twin boundary.

The observation that both the octahedral tilt twinning and the compositional modulation repeat with the same periodicity suggests an intimate link between the two, raising the intriguing possibility that the periodicity and/or pattern of the superlattice can be manipulated by changing the tolerance factor. Decreasing the tolerance factor, with respect to the ~0.95 value of $NaLaMgWO_6$, can be accomplished by substituting smaller rare-earth ions for La^{3+}, or larger divalent ions for Mg^{2+}. Well characterized examples of this type of substitution include $NaLaMnWO_6$ (τ = 0.930), $NaNdMnWO_6$ (τ = 0.918) and $NaTbMnWO_6$ (τ = 0.906).[13] In all three compounds, the smaller tolerance factor leads to in-phase rotations of the octahedra about the c-axis ($a^-a^-c^+$ tilting). The additional rotations appear to prevent octahedral tilt twinning and suppress superlattice formation.

The effect of increasing the tolerance factor has not previously been explored. Among $AA'BB'O_6$ perovskites reported in a recent review, the three compounds with the largest tolerance factors are $KLaMgTeO_6$ (τ = 1.010), $KLaMgWO_6$ (τ = 1.010), and $KLaMnWO_6$ (τ = 0.986).[14] Among these three, $KLaMnWO_6$ is perhaps the best candidate for further study. The $AA'MnWO_6$ perovskites are quite stable, and interesting patterns of tilting are often found when the tolerance factor lies between 0.97 and 1.00. A previous study on $KLaMnWO_6$ confirmed the expected layered ordering of the A-site cations and rock-salt ordering of the B-site cations.[13] Furthermore, peaks were reported in the neutron powder diffraction pattern that could not be accounted for by simple patterns of cation ordering or octahedral tilting, suggesting the presence of octahedral tilt twinning.

We present here a study of $KLaMnWO_6$ by selected area electron diffraction (SAED), high-resolution transmission electron microscopy (HRTEM), scanning transmission electron microscopy (STEM), electron energy loss spectroscopy (EELS), synchrotron powder X-ray diffraction (XRD), and neutron powder diffraction (NPD). These combined techniques reveal a complex superlattice structure in $KLaMnWO_6$.

2. Experimental Section

$KLaMnWO_6$ was prepared by the ceramic method using K_2CO_3 (Baker 99.9%), La_2O_3 (G. Frederick Smith 99.99%), and $MnWO_4$. The $MnWO_4$ was prepared from MnO (Cerac 99.9%) and WO_3 (Cerac 99.99%). A 5% excess of K_2CO_3 was used to account for the high-temperature volatility of this substance. Stoichiometric amounts of the reactants were ground together and heated at 1000 °C under a dynamic flow of forming gas (5% H_2, 95% N_2) for 8 h. The HRTEM images of this sample showed an irregular pattern. Therefore, the sample was annealed under the same conditions for an additional 24 h, after which the HRTEM image showed that the superstructure ordering had become much more regular.

Synchrotron X-ray powder diffraction data were collected at the ESRF on the high-resolution powder diffractometer ID31. Neutron powder diffraction data were collected at the Institut Laue-Langevin using the high resolution diffractometer D2B. The wavelength of the synchrotron beam was ~0.4 Å, whereas the wavelength of the neutron beam was 1.594 Å. Refinements of the synchrotron data were done using the Topas Academic[15]

(11) Lufaso, M. W.; Barnes, P. W.; Woodward, P. M. *Acta Crystallogr., Sect. B* **2006**, *62*, 397.
(12) King, G.; García-Martín, S.; Woodward, P. M. *Acta Crystallogr., Sect.* **2009**, *65*, 676.
(13) King, G.; Thimmaiah, S.; Dwivedi, A.; Woodward, P. M. *Chem. Mater.* **2007**, *19*, 6451.
(14) King, G.; Woodward, P. M. *J. Mater. Chem.* **2010**, *20*, 5785.
(15) *Topas Academic, General Profile and Structure Analysis Software for Powder Diffraction Data*; Bruker AXS: Karlsruhe, Germany, 2004.

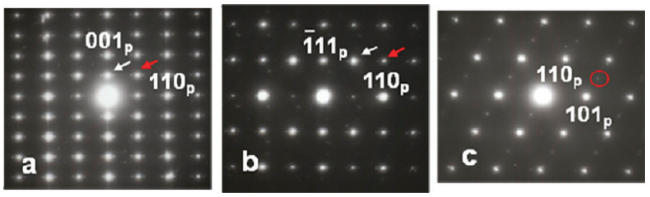

Figure 2. SAED patterns of a $KLaMnWO_6$ crystal along the (a) $[\bar{1}10]_p$, (b) $[\bar{1}1\bar{2}]_p$, and (c) $[\bar{1}11]_p$ zone axes.

program while refinements of neutron data were performed using the GSAS[16,17] software package.

For transmission electron microscopy the samples were ground in *n*-butyl alcohol and ultrasonically dispersed. A few drops of the resulting suspension were deposited in a carbon-coated grid. SAED studies were performed with an electron microscope (JEOL 2000FX) (double tilt ±45°) working at 200 kV. HRTEM and scanning TEM-electron energy-loss spectroscopy (STEM-EELS) studies were carried out with a JEM 3000F microscope operating at 300 kV (double tilt ±20°) (point resolution 1.7 Å), fitted with an ENFINA 1000 spectrometer and a JEOL annular dark field (ADF) detector. The STEM images were acquired with a collection angle of ~30 mrad. The spectral data sets were acquired as line scans, with an electron probe size diameter of ~0.3 nm, a collection time of 2 s, a dispersion of 0.5 eV/pixel, and a collection semiangle $\beta \approx 8.9$ mrad. The background under each individual spectrum was subtracted following a power-law model.[18]

3. Results

3.1. Transmission electron microscopy. Figure 2 shows SAED patterns of $KLaMnWO_6$ along different zone axes, where each pattern is indexed according to the ideal perovskite structure. As expected, superlattice reflections related to either *A* or *B* cation ordering appear in all patterns. The $1/2(001)_p$ and $1/2(021)_p$ reflections, indicated by white arrows in the patterns of the $[\bar{1}10]_p$ and $[1\bar{1}2]_p$ zone axes, respectively, are associated with layered-type ordering of K^+ and La^{3+} ions. The $1/2(111)_p$ and $1/2(131)_p$ reflections, indicated by red arrows, are associated with rock-salt ordering of Mn^{2+} and W^{6+} ions. The latter two reflections can also arise from out-of-phase octahedral tilts,[19−21] but in this case most of the intensity of these reflections is coming from rock-salt cation ordering.

The presence of $1/2(ooe)$ $h \neq k$ reflections such as $1/2(312)_p$, indicated by the red circle in the $[1\bar{1}\,\bar{1}]_p$ zone axis pattern, can arise from in-phase tilting of the octahedra about the *c*-axis.[21] However, the presence of cation ordering in combination with out-of-phase tilting of the octahedra leads to cation displacements, which can also account for the appearance of these reflections. Thus we are not able to definitively identify the octahedral tilting pattern from the electron diffraction patterns.

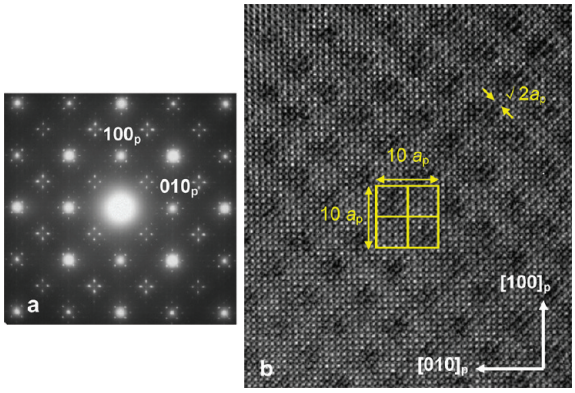

Figure 3. (a) SAED pattern and (b) HRTEM image corresponding to the $[001]_p$ zone axis of a $KLaMnWO_6$ crystal.

Figure 3a shows the SAED pattern along $[001]_p$ zone axis. There are satellite reflections along $[100]_p$, $[010]_p$, $[110]_p$, and $[1\bar{1}0]_p$ directions, which reveal a modulation of the crystal structure. The distance between satellites corresponds to the periodicity of the modulation, which in this case is $10a_p$ along $[100]_p$ and $[010]_p$. Modulation of the crystal structure is also observed in HRTEM. Figure 3b shows the HRTEM image corresponding to the $[001]_p$ zone axis. Contrast differences formed by dark areas intercalated with bright areas, forming a chessboard pattern, are observed. In addition, lattice fringes along $[110]_p$ indicate a $\sqrt{2}a_p$ periodicity along this direction, which in perovskites is usually associated with tilting of the octahedra. The size of the dark and bright regions ($\sim 5a_p \times \sim 5a_p$) is consistent with the $10a_p$ periodicity derived from the superlattice reflections in the SAED patterns.

On the basis of prior studies of perovskite-related phases, such as $NaLaMgWO_6$[7] and the $Nd_{2/3-x}Li_{3x}TiO_3$ system,[6,8,9,22] we hypothesize that the modulations seen in Figure 3 arise from either a periodic modulation of the composition, or periodic twinning of the octahedral tilts, or both. The HAADF-STEM technique (also called Z-contrast STEM) is a powerful tool to probe samples for compositional modulations, because the contrast seen in HAADF-STEM images is directly related to Z.[23] Figure 4 shows an HAADF-STEM image of $KLaMnWO_6$ along the $[001]_p$ zone axis. As in the HRTEM images, contrast differences formed by dark and bright areas leading to a chessboard-type pattern can be seen. This image suggests the existence of a compositional modulation of the crystal structure.

As discussed in earlier studies of compositional modulations in $NaLaMgWO_6$, the contrast seen in HRTEM and HAADF-STEM images can arise from modulations of the *A*-site cations, or the *B*-site cations or a combination of both.[7,12] In an attempt to differentiate between these three possibilities, we acquired STEM-EELS line-scans along different directions collecting at

(16) Toby, B. H. *J. Appl. Crystallogr.* **2001**, *34*, 210.
(17) Larson., A. C.; Von Dreele, R. B. *GSAS: General Structure Analysis System*; Report LAUR 86-748; Los Alamos National Laboratory: Los Alamos, NM, 2004.
(18) Egerton, R. F. *Electron Energy-Loss Spectroscopy in the Electron Microscope*; Plenum Press: New York, 1996.
(19) Glazer, A. M. *Acta Crystallogr., Sect. B* **1972**, *28*, 3384.
(20) Glazer, A. M. *Acta Crystallogr., Sect. A* **1975**, *31*, 756.
(21) Woodward, D. Y.; Reany, I. M. *Acta Crystallogr., Sect. B* **2005**, *61*, 387.
(22) García-Martín, S.; García-Alvarado, F.; Robertson, A. D.; West, A. R.; Alario-Franco, M. A. *J. Solid State Chem.* **1997**, *128*, 97.
(23) Nellist, P. D. Scanning Transmission Electron Microscopy. In *Science of Microscopy*; Hawkes, P., Spence, J. C. H., Eds.; Springer: New York, 2007.

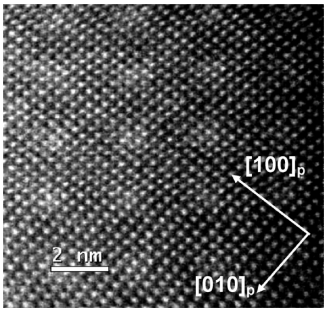

Figure 4. HAADF-STEM image of a $KLaMnWO_6$ crystal along the $[001]_p$ zone axis.

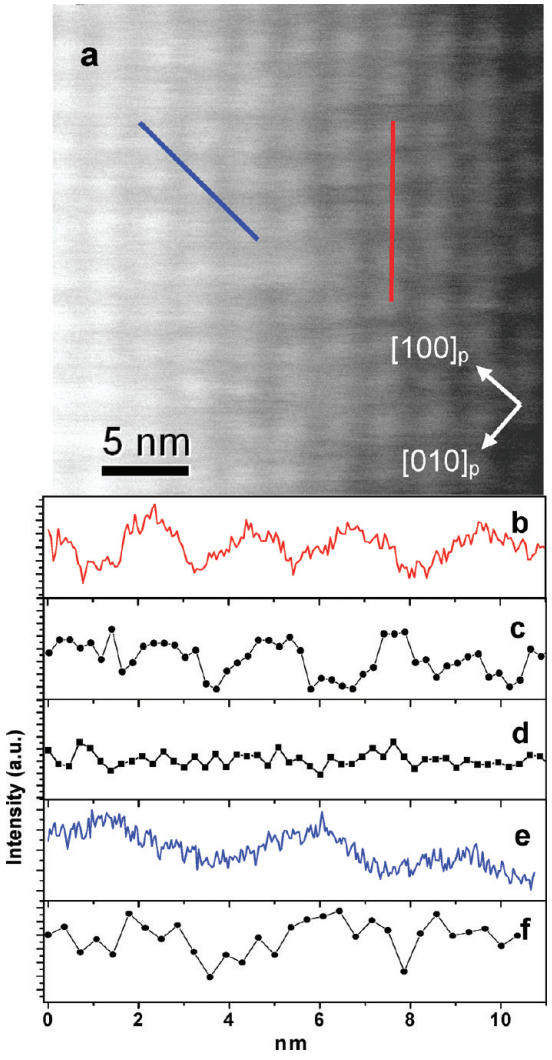

Figure 5. (a) HAADF-STEM image of a $KLaMnWO_6$ crystal along the $[001]_p$ zone axis, (b) contrast intensity variation of the HAADF-STEM image from the STEM-EELS line scan along $[110]_p$ indicated by the red line in the image, (c) variation of the intensity of the La $M_{4,5}$ edge signal, obtained from the STEM-EELS line scan along $[110]_p$ (d) variation in the intensity of the Mn $L_{2,3}$ edge signal, obtained from the STEM-EELS line scan along $[110]_p$, (e) contrast intensity variation of the HAADF-STEM image from the STEM-EELS line scan along $[100]_p$ indicated by the blue line in the image, and (f) variation of the intensity of the La $M_{4,5}$ edge signal, obtained from the STEM-EELS line scan along $[100]_p$.

both the La-$M_{4,5}$ and the Mn-$L_{2,3}$ edges. As shown in Figure 5, a periodic variation of the La content, similar to the variation seen in the HAADF-STEM image, is observed. In contrast, the Mn content seems to be uniform.

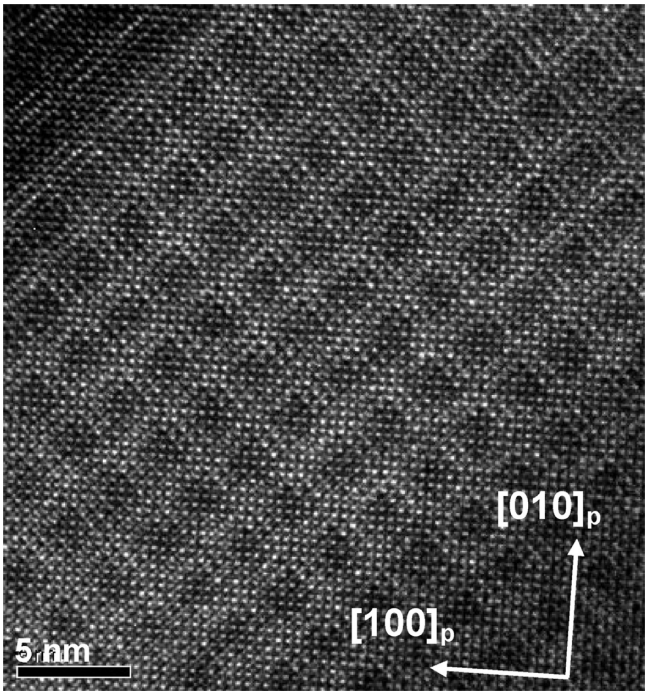

Figure 6. HRTEM image corresponding to the $[001]_p$ zone axis of a KLaMnWO6 crystal.

Line scans along different directions always indicate modulation of the La content and uniformity of the Mn content. These results provide strong evidence that a compositional modulation is associated with the La/K sublattice, but not with the Mn/W sublattice. Energy filtered transmission electron microscopy (EFTEM) images taken at the La-$M_{4,5}$ edge and the Mn-$L_{2,3}$ edge also support the idea that the compositional modulation is associated with the La/K sublattice. La-$M_{4,5}$ jump-ratio images show contrast differences while Mn-$L_{2,3}$ jump-ratio images do not (see Figure 1SI in the Supporting Information).

The superlattice reflections seen in the SAED patterns around $1/2(110)_p$ and equivalent positions of the $[001]_p$ zone axis (Figure 3a) are reminiscent of patterns seen in related perovskites.[6−8] In previous studies, these features have been ascribed to the formation of four antiphase domains due to twinning of the octahedral tilt system,[12,24−26] suggesting that octahedral tilt twinning is also present in $KLaMnWO_6$. This hypothesis is supported by HRTEM images taken along the $[001]_p$ zone axis in crystals of appropriate thickness, as shown in Figure 6. Fringes that likely arise from tilt twinning appear along $[110]_p$ and $[\bar{1}10]_p$, forming bright stripes along these two perpendicular directions. These stripes are superimposed with the contrast differences associated with the La/K compositional modulation.

3.2. Synchrotron X-ray Powder Diffraction. The synchrotron X-ray powder diffraction pattern (Figure 7) could be indexed using the tetragonal space group *P*4/*nmm* with

(24) Alario-Franco, M.Á.; Grey, I. E.; Joubert, J. C.; Vincent, H.; Labeau, M. *Acta Crystallogr., A* **1982**, *38*, 177.
(25) Labeau, M.; Grey, I. E.; Joubert, J. C.; Vincent, H.; Alario-Franco, M. Á . *Acta Crystallogr., A* **1982**, *38*, 753,
(26) García-Martín, S.; Alario-Franco, M. Á . *J. Solid State Chem.* **1999**, *148*, 93.

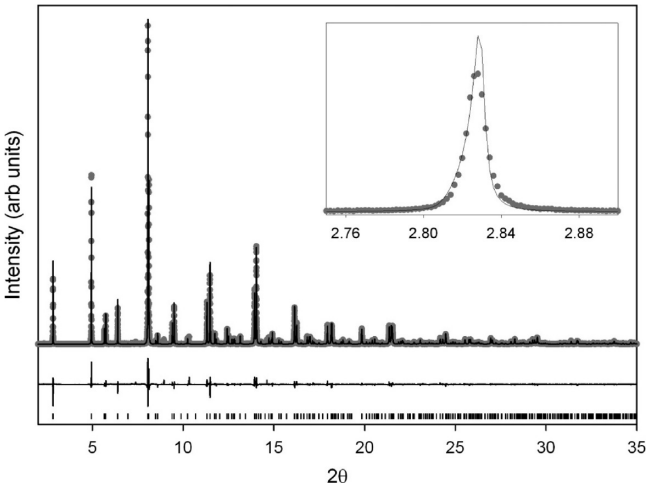

Figure 7. Results of the Rietveld refinement of the synchrotron XRD data using space group $P4/nmm$. The inset shows the fit to the 001 peak. Gray circles are experimental data points, the solid line is the calculated fit, and the difference curve is shown beneath.

$a = \sqrt{2}a_p$ and $c = 2a_p$. According to a prior group theoretical analysis, this space group and unit cell are appropriate for perovskites with both rock salt *B*-site ordering and layered *A*-site ordering, provided there is no octahedral tilting.[27] There were a few very weak additional reflections that were not indexed by this space group, but these peaks had different profiles and did not appear at positions corresponding to the supercells derived from SAED. Therefore, we attribute their presence to a trace amount of an unidentified secondary phase. No supercell reflections corresponding to the larger unit cell derived from SAED could be detected. This highlights the hazard of using only XRD data for the structure determination of $AA'BB'O_6$ perovskites, even when the XRD data is of very high quality.

The lattice parameters refined to $a = 5.66023(2)$ Å, $c = 8.12127(4)$ Å. The Rietveld refinement performed in this space group gives an R_{wp} of 14.29. The relatively high R_{wp} value provides an indication that this structural model is not quite correct. One of the most poorly fit peaks is the 001 peak, shown in the inset of Figure 7. Because this peak is associated with K/La ordering, the inability to properly fit it suggests that simple layered ordering of K^+ and La^{3+} is not a completely adequate description of the structure.

3.3. Neutron Powder Diffraction. The electron microscopy results strongly suggest the presence of octahedral tilt twinning. To confirm this hypothesis and quantitatively model the octahedral tilting we turned to neutron diffraction. Neutron diffraction is a powerful probe of octahedral tilting in perovskites, due to its sensitivity to the oxygen positions. In previous studies of $NaLaMgWO_6$[12] and $Nd_{2/3-x}Li_{3x}TiO_3$[28] neutron diffraction studies have been instrumental in modeling the complex patterns of octahedral tilting.

The NPD pattern of $KLaMnWO_6$, like those of $NaLaMgWO_6$ and $Nd_{2/3-x}Li_{3x}TiO_3$, possesses satellite

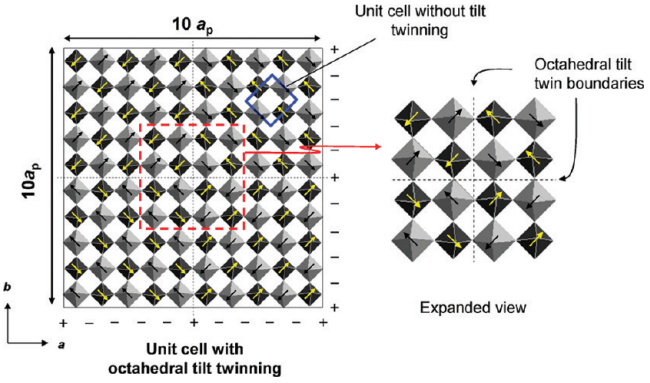

Figure 8. Unit cell used to model octahedral tilting in $KLaMnWO_6$. The − and + symbols indicate out-of-phase and in-phase octahedral tilting, respectively. The arrows show the direction that the apex oxygen of the octahedron moves as a result of tilting. An expanded view of the central region of the unit cell is shown on the right. The K^+ and La^{3+} ions have been omitted for clarity, and even though the unit cell is two octahedra high, only the lower layer is shown here.

reflections that cannot be accounted for with conventional octahedral tilt models. Since the HRTEM and SAED patterns suggest a superstructure along both $[100]_p$ and $[010]_p$, it is logical to assume that the tilt twinning is also two-dimensional with perpendicular twin boundaries. If there is twinning in two directions there must be octahedral tilting in at least two directions as well. Combining tilts about the *a* and *b* axes with a tilt about the *c*-axis ($a^-a^-c^+$ tilting) results in unreasonable distortions of the octahedra at the twin boundaries, as discussed in ref 12. This leaves the $a^-a^-c^0$ tilt system as the most likely choice for the underlying tilt system on which tilt twinning occurs.

The $10a_p \times 10a_p \times 2a_p$ unit cell suggested by electron diffraction is too large for unconstrained Rietveld refinements. However, it is possible to build a model structure that can be used to explain the observed diffraction data. Based on the electron microscopy results, in-phase tilts ("octahedral tilt twin boundaries") were inserted every five octahedra along both the *x* and *y*-directions (Figure 8). The atomic positions were estimated using the following assumptions, based on the structures of ordered AA'-$MnWO_6$ perovskites that show conventional octahedral tilting.[12]

(1) The oxygen ions are assumed to define undistorted octahedra, the sizes of the octahedra were determined by bond valence calculations.

(2) Each Mn^{2+} ion is assumed to lie at the centroid of its octahedron.

(3) Each W^{6+} ion is displaced by 0.15 Å from the centroid of its octahedron along the *c*-axis toward the K^+ layer.[13]

(4) The *A*-site cations are assumed to lie at the same positions they would occupy in the ideal perovskite structure.

The symmetry of the resulting structure is tetragonal, possessing $P\bar{4}2m$ space group symmetry. There are 1,000 atoms in the unit cell, out of which 152 are crystallographically independent. The resulting structural model is shown in Figure 8.

(27) Knapp, M. C.; Woodward, P. M. *J. Solid State Chem.* **2006**, *179*, 1076.
(28) Guiton, B. S.; Wu, H.; Davies, P. *Chem. Mater.* **2008**, *20*, 2860.

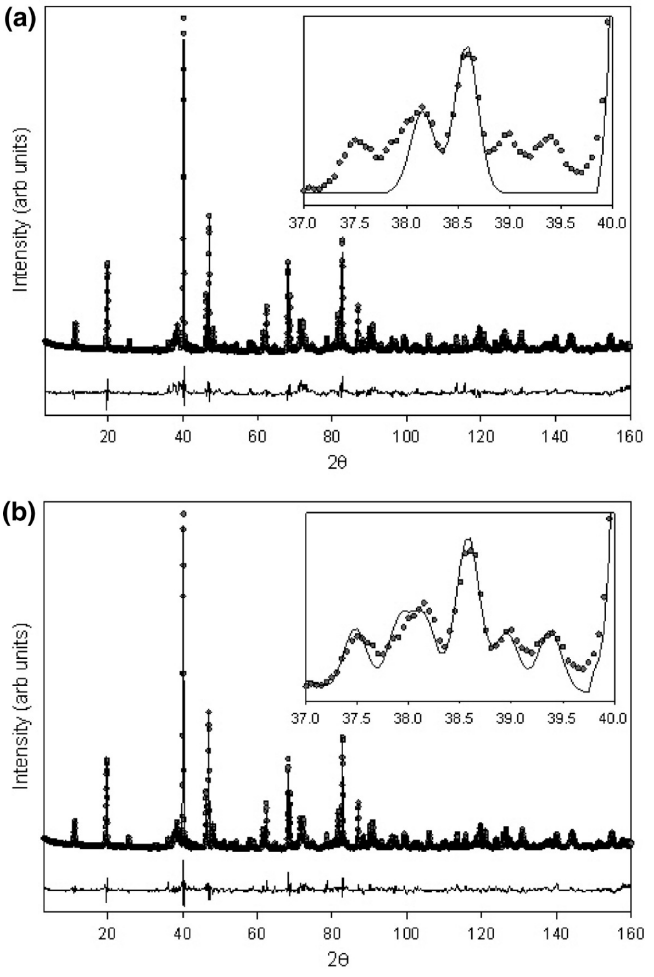

Figure 9. (a) Results of the Rietveld refinement of the NPD data using space group *P*4/*nmm*, which does not include tilt twinning. The inset shows a region where superlattice peaks are most pronounced. (b) Results of the Rietveld refinement when the supercell that includes tilt twinning is included. Gray circles are experimental data points, the solid line is the calculated fit, and the difference curve is shown beneath.

Simulated NPD patterns using this model exhibit satellite reflections at the correct 2θ positions. A Rietveld refinement was performed to see how well the model could reproduce the intensities. As stated earlier, the size of the unit cell prevents us from performing an unconstrained Rietveld refinement. Therefore, only the scale factor, unit-cell dimensions, background, peak shape, and displacement parameters were allowed to refine. Atoms corresponding to the same element were constrained to have the same displacement parameters. The atomic positions were fixed by the model. Initial refinements were not able to model the intensities of some reflections accurately, suggesting that some of the assumptions made in constructing the model are not valid.

Because the La^{3+} and K^+ ions differ significantly in size, the next step was to relax our assumption that the oxygen ions define undistorted octahedra. To account for the La/K size difference, the oxygen atoms that lie between the La^{3+} and K^+ layers were shifted along the *c*-axis toward the smaller La^{3+} ion by 0.18 Å. The magnitude of this distortion was estimated by refining in the *P*4/*nmm* subcell and observing the displacements of these anions. This led to a significant improvement to the fit to the point where intensities were reasonably well accounted for. Refinements were carried out using models with a number of different tilt angles. Tilt angles of 6 and 7° were found to give the best fits, implying the true tilt angle lies somewhere between these two values. The χ^2 of the best fit was 6.29. Figure 9 shows how the fit obtained using the model with a 7° tilt angle compares with a fit that does not include tilt twinning. The unit cell parameters refined to be 40.0637(7) Å × 40.0637(7) Å × 8.1306(3) Å. Crystallographic data are given in the Supporting Information.

4. Discussion

As with other $AA'BWO_6$ perovskites the K^+ and La^{3+} ions order into alternating layers in $KLaMnWO_6$. This ordering, along with the rock salt ordering of the Mn^{2+} and W^{6+} ions, can readily be seen with X-ray, neutron or electron diffraction. In addition we find a $10a_p \times 10a_p \times 2a_p$ superlattice that consists of a compositional modulation of the *A*-site cation occupancy, coupled with a twinning of the octahedral tilting. Taking into account our STEM-EELS results, we propose a model for the compositional modulation similar to the model proposed for $NaLaMgWO_6$.[7] In this model the La^{3+} layers are fully occupied and continuous throughout the crystal, but the occupancy of the K^+ layers is modulated. In the La-poor domains the K^+ sites are essentially fully occupied and the intended stoichiometry is maintained, whereas in the La-rich domains K^+ vacancies are compensated for by La^{3+} ions sitting on the K^+ sites. To maintain charge balance, there must be one extra La^{3+} ion for every three K^+ vacancies, giving a stoichiometry of $K_{1-3x}La_{1+x}MnWO_6$ (see Figure 10). The nonstoichiometry needed for a compositional modulation may help to explain the trace amount of a secondary phase detected by synchrotron powder X-ray diffraction.

Although the electron microscopy studies clearly demonstrate a periodic compositional modulation, it is difficult to precisely define the abruptness of the modulation or the relationship between La-rich and stoichiometric regions with respect to the octahedral tilt twin boundaries (i.e., the in-phase octahedral tilts). Two possible models are shown in Figure 10. The appeal of model 1 is based on the idea that the *A*-site coordination environment will be slightly different at the tilt twin boundary than it is away from the boundary. If this different environment is favorable for incorporating either La^{3+} ions or vacancies within the K^+ layers, the La-rich regions may prefer to nucleate in the vicinity of the in-phase tilts. On the other hand, if the in-phase tilts form in order to relieve strains associated with the subtly different lattice parameters of the La-rich and stoichiometric regions, then model 2 seems more plausible.

In an attempt to differentiate between models 1 and 2 let us return to the HAADF-STEM image shown in Figure 5a. That image is reproduced in Figure 11 with the octahedral tilt twin boundaries and unit cell derived from

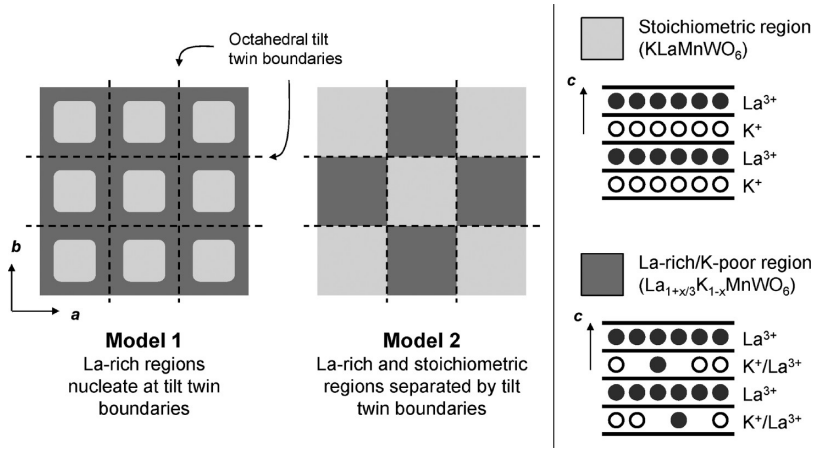

Figure 10. Two models for defining the relationship between compositional modulation and octahedral tilt twinning.

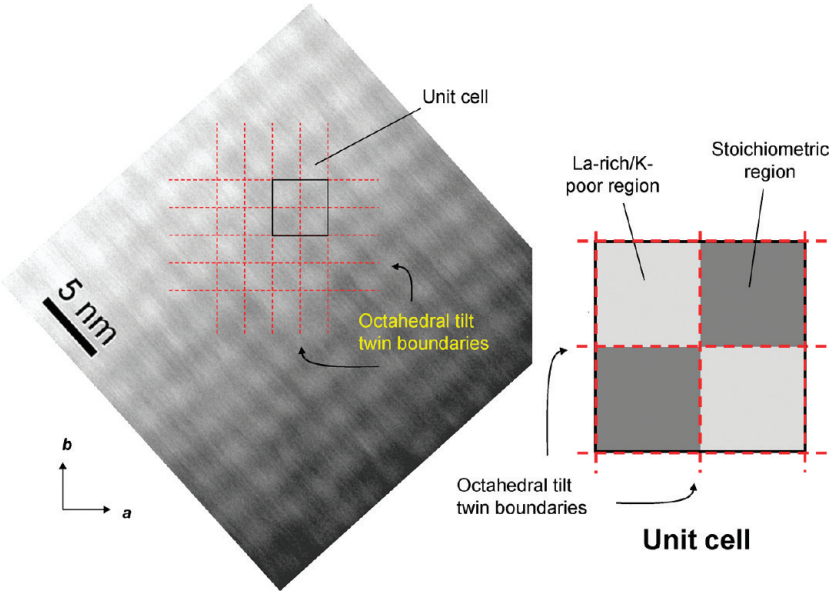

Figure 11. HAADF-STEM image from Figure 5 with the octahedral tilt twin boundaries and unit cell superimposed.

neutron diffraction superimposed. The HAADF-STEM image is clearly in better agreement with model 2. Although this does not rule out a modulation that is a hybrid between models 1 and 2, it does suggest that the in-phase tilts form in order to alleviate lattice mismatch between La-rich and stoichiometric domains.

An interesting feature of this modulation is the tetragonal symmetry of the supercell, despite the fact that $a^-a^-c^0$ tilting would produce monoclinic $P2_1/m$ symmetry in the absence of octahedral tilt twinning. The tetragonal lattice parameters derived from XRD could be taken as a sign that octahedral tilting is absent, but as the analysis here shows this assumption would be erroneous. Because the additional supercell reflections that arise from the octahedral tilt twinning can only be seen with electron and neutron diffraction it is not unreasonable to suggest that similar superstructures have gone undetected in other $AA'BB'O_6$ perovskites.[13] This observation could help to explain why perovskites like $NaCeMnWO_6$ and $NaPrMnWO_6$ were found by XRD analysis to have metrically tetragonal lattice parameters despite the fact that their tolerance factors are much too small for them to be stable without octahedral tilting.[29,30] The tetragonal metrics of these phases could be an indication that two-dimensional tilt twinning is also occurring in these compounds.

Despite the fact that compositional modulations in complex perovskites were not documented prior to 2007 these complex superlattice structures seem to be rather prevalent in $A_{2-x}A'_xBB'O_6$ perovskites.[6] However, there are many gaps in our understanding of this phenomenon. One of the most important questions to be answered is what drives the spontaneous formation of such complex structures. Regarding this question, it is worth mentioning recent studies on systems with pseudospinodal decomposition into two phases, leading to nanoscale

(29) King, G.; Wayman, L. M.; Woodward, P. M. J. *Solid State Chem.* **2009**, *182*, 1319–1325.
(30) King. G. Ph.D. Dissertation, The Ohio State University, Columbus, OH, 2010.

chessboard structures.[31,32] Coherent strain due to crystal lattice mismatch between phases with different compositions is thought to play an important role in stabilizing formation of these complex arrangements. Furthermore, the kinetics involved with ion migration must be sufficiently fast that the compositionally modulated nanostructure can form at temperatures where it is thermodynamically stable. It is interesting to note that other examples of octahedral tilt twinning, $Th_{1/4}NbO_3$,[24,25] $Nd_{2/3-x}Li_{3x}TiO_3$,[6,8] and $Na_{0.5}Bi_{0.5}TiO_3$[33,34] also possess two different ions on the *A*-sites (if we count vacancies as a type of ion) and a d^0 ion on the *B*-site.

Our results on complex superlattice arrangements of both $KLaMnWO_6$ and $NaLaMgWO_6$[7,12] are in line with this view. Optimal thermodynamic and kinetic conditions seem to be essential for the modulation of the crystal structure. In fact, as it is mentioned in the Experimental Section, our $KLaMnWO_6$ samples initially showed an irregular pattern characteristic of an incipient modulation. Only after annealing for 24 h does the nanochessboard order fully develop.

Another interesting question is why $KLaMnWO_6$ adopts a two-dimensional chessboard lattice while $NaLaMgWO_6$ prefers one-dimensional stripes. Perhaps as the tolerance factor decreases, and the magnitude of the octahedral tilts increases, there is a crossover from a 2D to a 1D pattern of octahedral tilt twinning and the compositional modulation simply follows suit. Apparently further decreases in the tolerance factor, as seen in $NaLnMnWO_6$ (*Ln* = La, Nd, Tb), trigger a tilt about the third axis ($a^-a^-c^0$ to $a^-a^-c^+$) and the octahedral tilt twinning is lost altogether removing any stabilization of the compositional modulation.

(31) Ni, Y.; Khachaturyan, A. G. *Nat. Mater.* **2009**, *8*(5), 410.
(32) Ni, Y.; Rao, W.; Khachaturyan, A. G. *Nano Lett.* **2009**, *9*(9), 3275.
(33) Dorcet, V.; Trolliard, G.; Boullay, P. *Chem. Mater.* **2008**, *20*, 5061.
(34) Dorcet, V.; Trolliard, G.; Boullay, P. *J. Magn. Magn. Mater.* **2009**, *321*, 1758.

Conclusions

A detailed study of the structure of the perovskite $KLaMnWO_6$ reveals a self-assembled nanostructured architecture which consists of two types of domains arranged like a chessboard. Compositional modulation within the *A*-cation sublattice is confirmed by HAADF-STEM and EELS. We suggest two domains of the $K_{1-3x}La_{1+x}MnWO_6$ system, both with average $\sqrt{2}a_p \times \sqrt{2}a_p \times 2a_p$ unit cells but with different La/K content. In combination with the compositional modulation, the octahedral tilts form a two-dimensional network of periodic twin boundaries (in-phase tilts on a background of out-of-phase tilts) that run perpendicular to the layered K/La ordering. The octahedral tilt twinning appears to be important for alleviating epitaxial strain that arises from crystallographic mismatch between domains of different compositions. The combination of the compositional modulation and the tilt twinning leads to a tetragonal superlattice structure with cell dimensions $10a_p \times 10a_p \times 2a_p$.

Acknowledgment. The authors thank the Institut Laue-Langevin, Grenoble, France, for the allocation of neutron beam time through the Easy Access System (http://www.ill.eu/users/applying-for-beamtime/easy−easy-access-system/) and the European Synchrotron Radiation Facility, Grenoble, France, for the allocation of beamtime. The authors are grateful to E. Suard (ILL) and A. Fitch for their assistance during the data collection. We also thank the Microscopy Centre's Luis Bru from UCM for technical assistance. S.G-M. and E.U-G. thank the Spanish MEC for funding Project MAT2007-64486-C07-04 and CAM for Projects MATERYENER S505/PPQ/0358 and P2009/PPQ-1629. G.K. and P. M.W. thank the National Science Foundation (Award DMR-0907356) for financial support.

Supporting Information Available: Energy-filtered TEM images (PDF) and crystallographic information (CIF). This material is available free of charge via the Internet at http://pubs.acs.org.